Direct experimental evidence of hybridization of Pb states with O 2*p* states in ferroelectric perovskite oxides

J. C. Jan,[a] H. M. Tsai, C. W. Pao, J. W. Chiou, K. Asokan,[b]
K. P. Krishna Kumar, and W. F. Pong[c]
Department of Physics, Tamkang University, Tamsui, Taiwan 251, Republic of China

Y. H. Tang and M.-H. Tsai
Department of Physics, National Sun Yat-Sen University, Kaohsiung, Taiwan 804, Republic of China

S. Y. Kuo
Precision Instrument Development Center, National Science Council, Hsinchu, Taiwan 300, Republic of China

W. F. Hsieh
Department of Photonics and Institute of Electro-Optical Engineering, National Chiao Tung University, Hsinchu, Taiwan 300, Republic of China

(Received 10 March 2005; accepted 25 May 2005; published online 28 June 2005)

This work presents the O *K*- and Ti $L_{3,2}$-edge x-ray absorption near-edge structure (XANES) spectra of $Pb_xSr_{1-x}TiO_3$ (P_xSTO) and $Ba_xSr_{1-x}TiO_3$ (B_xSTO) compounds with various Pb and Ba concentrations. The result provides direct evidence that the Pb–O bonding strongly affects O 2*p*–Ti 3*d* hybridization in the TiO_6 octahedron of P_xSTO. In contrast, the Ba–O bonding does not substantially affect O 2*p*–Ti 3*d* hybridization in B_xSTO. The Ti L_3-edge XANES spectra show the splitting of the e_g band for P_xSTO with $x \gtrsim 0.5$, which provides an evidence of Pb-induced tetragonal distortion in the TiO_6 octahedron. In contrast, e_g band splitting is absent in B_xSTO. © *2005 American Institute of Physics*. [DOI: 10.1063/1.1988984]

Ferroelectric perovskite oxides of the ABO_3-type including $BaTiO_3$ (BTO), $SrTiO_3$ (STO), and $PbTiO_3$ (PTO) are important materials because of their piezoelectric, pyroelectric and dielectric properties.[1,2] Interestingly, these materials have tunable properties over a wide range of mixed solid solutions doped with various cations.[1] A characteristic unit cell of these perovskites contains a TiO_6 octahedron. Collective polarization of the TiO_6 octahedra is believed to determine the ferroelectric characteristics.[3–6] X-ray absorption near-edge structure (XANES) measurements and first-principles calculations have been used to elucidate the role of alkaline-earth metals in perovskites,[7–9] which showed that A cations influenced the coupling between Ti and O ions and is responsible for tuning the ferroelectric properties. Kuo *et al.* determined the lattice constant from x-ray diffraction (XRD) data and observed a structural change from cubic to tetragonal (associated with an increase in the tetragonal distortion **c/a**) for $Pb_xSr_{1-x}TiO$ (P_xSTO) at $x=0.5$ (Ref. 10) and for $Ba_xSr_{1-x}TiO_3$ (B_xSTO) at $x=0.7$.[11] They also carried out Raman measurements for P_xSTO and B_xSTO and found that the splitting of longitudinal optical (LO) and transverse optical (TO) modes became stronger as the Pb content in the tetragonal phase of P_xSTO increases, while the splitting became weaker as the Ba content in B_xSTO increases. These results were explained by the covalent Pb–O bonding in P_xSTO and ionic Ba–O bonding in B_xSTO.[10–12] The present study is intended to understand the electronic structures of P_xSTO and B_xSTO solid solutions by O *K*- and Ti $L_{3,2}$-edges XANES measurements to elucidate the role of Pb and Ba ions in $M_xSr_{1-x}TiO_3$ (M=Pb and Ba).

Room-temperature XANES spectra at the O *K*- and Ti $L_{3,2}$-edges were recorded using a high-spherical grating monochromator beamline in fluorescence and sample drain current modes, respectively, at the National Synchrotron Radiation Research Centre, Taiwan. P_xSTO and B_xSTO (where x is varied from 0 to 1) solid solutions were prepared by the sol-gel method and characterized by XRD. The details of the preparation and characterization of these samples have been reported elsewhere.[10,11]

Figures 1 and 2 present the normalized O *K*-edge XANES spectra of P_xSTO and B_xSTO ($x=0$ to 1) compounds, respectively, and reference TiO_2. These spectra were divided by the incident intensity I_0 and normalized to the same area in the energy range between 550 and 560 eV (not fully shown). The main spectral features in the spectra of PTO (BTO) in Fig. 1 (Fig. 2) are centered at ~531 (530.5), 532, 534 (533.5), and 537 (537) eV and are labeled as A_1 (A_2) to D_1 (D_2), respectively. These features correspond to transitions from the O 1*s* core state to the unoccupied O 2*p*-derived states. According to first-principles calculations for P_xSTO (Ref. 13) and B_xSTO (Ref. 9) these states are hybridized states between O 2*p* and relatively narrow 3*d* and broader 4*sp* bands of the Ti ion and Pb 6*sp* and Sr 4*d*/(Ba 5*d*) bands. Specifically, spectral features A_1, C_1, and B_1 are attributable to hybridized states between O 2*p* and Ti 3*d* and Pb 6*sp*, while features A_2 and C_2 are associated with O 2*p*–Ti 3*d* hybridized states. A similar two-peak structure (t_{2g} and e_g states) at the threshold of the O *K*-edge is commonly obtained from 3*d*-transition metal oxides.[14] Feature D_1 (D_2) in the spectra of P_xSTO (B_xSTO) is attributable

[a]Present address: National Synchrotron Radiation Research Center, Hsinchu, Taiwan 300, Republic of China.
[b]Permanent address: Nuclear Science Centre, Aruna Asaf Ali Marg, New Delhi-110067, India.
[c]Author to whom correspondence should be addressed; electronic mail: wfpong@mail.tku.edu.tw

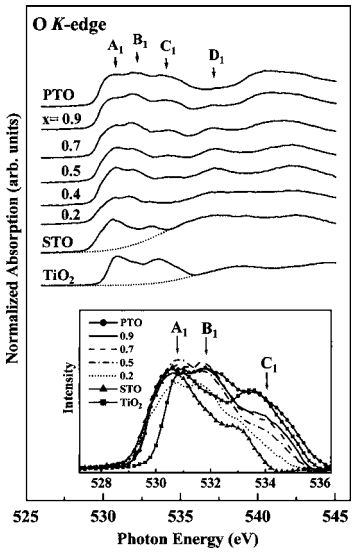

FIG. 1. Normalized O *K*-edge XANES spectra of the P_xSTO ($x=0-1$) samples. The dashed line represents a best-fitted Gaussian shape background. The inset shows the magnified near-edge feature after background subtraction.

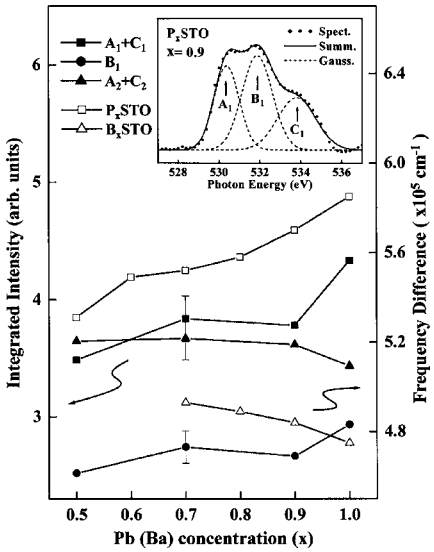

FIG. 3. Integrated intensities of A_1+C_1, B_1, and A_2+C_2 features in O *K*-edge XANES spectra as functions of the Pb (Ba) concentration. [The frequency difference data of P_xSTO (open squares) and B_xSTO (open triangles) are from Refs. 10 and 11, respectively]. The inset shows a magnified view of A_1, B_1, and C_1 features and fitted result of P_xSTO at $x=0.9$.

to the O $2p$ derived states hybridized with Sr $4d$ (Sr $4d$/Ba $5d$) orbitals. The insets of Figs. 1 and 2 show magnified near-edge features with the background subtracted to highlight intensity differences. The inset of Fig. 1 shows that feature B_1 emerges between features A_1 and C_1 when the Pb content is added. Furthermore, strong hybridization between O $2p$ and Ti $3d$/Pb $6sp$ states increases the number of unoccupied O $2p$ derived states and broadens the features for P_xSTO. In contrast, the general spectral line shapes and widths in the inset of Fig. 2 are very similar for B_xSTO because Ba and Sr ions have similar valence states. The similarity of the spectra of B_xSTO also shows that substitution of Sr by Ba insignificantly affects the Ti–O bonding in B_xSTO. Feature A_2 shifts slightly to lower energy as the Ba content increases. This trend is due to the fact that the electronegativity of Ba (0.89) is slightly less than that of Sr (0.95),[15] so that the average electronegativity of cations decreases and the negative effective charge of the O ion increases with the Ba content. The O *K*-edge XANES spectra of P_xSTO have more features than those of B_xSTO. This indicates that the Pb–O covalent bonding has additional contribution to the spectra and such result is consistent with the findings of Kuroiwa *et al.*[16] and also in agreement with the theoretical prediction of Cohen.[4]

Figure 3 plots the integrated intensities of A_1+C_1 (ranged from 528 to 532 eV and 532 to 536 eV, respectively), B_1 (ranged from 530 to 534 eV), and A_2+C_2 (ranged from 528 to 535 eV) absorption features attributable to O $2p-$Ti $3d$ and O $2p-$Pb $6sp$ derived states, respectively, as a function of the Pb (Ba) concentration in P_xSTO (B_xSTO). The inset of Fig. 3 shows a magnified view after background subtraction to better resolve A_1, B_1, and C_1 features of P_xSTO using the $x=0.9$ case as an example. Three best-fitted Gaussian peaks are used to represent A_1, B_1, and C_1 features. Figure 3 also compares the frequency difference between $TO[A_1(TO_1)]$ and $LO[A_1(LO_3)]$ as a function of the Pb (Ba) concentration from Refs. 10 and 11. Figure 3 demonstrates that the partial substitution of A cations, Sr, by Pb increases the number of unoccupied O $2p-$Ti $3d$ and O $2p-$Pb $6sp$ hybridized states when x increases from 0.5 to 1 in P_xSTO, which may suggest a charge transfer that increases the effective charges of Ti and, consequently, the attractive Coulomb potentials on Ti sites (Pb has a much larger electronegativity than Ti and Sr, so its effective charge is less likely to increase). This charge transfer causes the LO-TO splitting to increase with the Pb content in P_xSTO. In contrast, Fig. 3 reveals that the overall intensities of the sum of features of A_2 and C_2 drops slightly as the Ba content increases, which indicates a decrease of the number of unoccupied O $2p-$Ti $3d$ hybridized states and suggests a reduction of the effective charge that decreases the Coulomb force between O and Ti ions and, consequently, a slight decrease of the LO-TO splitting in B_xSTO. The ferroelectric property results from a detailed balance between the long-range Coulomb interaction and short-range forces.[4] Thus, the significant charge transfer in P_xSTO enhances the long-range Cou-

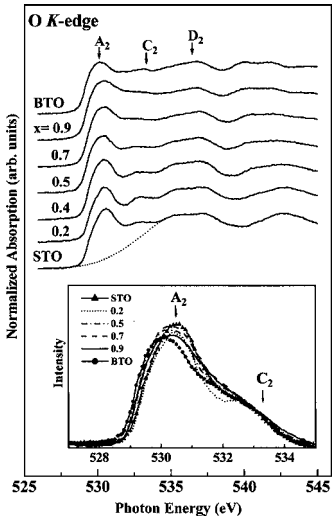

FIG. 2. Normalized O *K*-edge XANES spectra of the B_xSTO ($x=0-1$) samples. The dashed line represents a best-fitted Gaussian shape background. The inset shows the magnified near-edge feature after background subtraction.

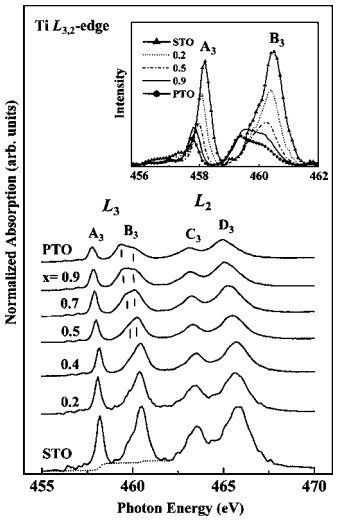

FIG. 4. Normalized Ti $L_{3,2}$-edge XANES spectra of P_xSTO. The inset presents the magnified A_3 and B_3 features after background subtraction.

lomb interaction and improves the ferroelectric characteristics.

Figures 4 and 5 present the Ti $L_{3,2}$-edge XANES spectra of P_xSTO and B_xSTO compounds, respectively. These spectra are split into L_3 and L_2 regions by the spin-orbit interaction in the Ti $2p$ core states[17–19] with a separation of ~5.5 eV. Each region contains t_{2g} and e_g splitting of approximately 2 eV caused by the crystal-field effect. The spectra in Fig. 4 contain four dominant features, of which the first two features, A_3 and B_3, correspond to the L_3-edge with t_{2g} and e_g symmetries, respectively. The other two features, C_3 and D_3, in the higher-energy region correspond to the L_2-edge with t_{2g} and e_g symmetries, respectively.[19,20] The crystal field due to the perfect O_h symmetry gives rise to two distinct t_{2g} and e_g bands. The lowering of the symmetry to D_{2d} causes e_g to split. Feature B_3 exhibits a splitting of approximately 0.5 eV (marked by the vertical lines in Fig. 4) for P_xSTO for $x \geqslant 0.5$, which suggests off-center displacement of the Ti ion. This splitting can be understood by the strong tetragonal distortion.[8] In contrast, as presented in Fig. 5, feature B_4 in the spectra of B_xSTO exhibits no clear splitting, which indicates that the tetragonal distortion **c/a** is insignificant for B_xSTO.[11] The insets of Figs. 4 and 5 highlight the splitting by subtracting the background using two arctangent functions shown by dashed lines. These two arctangent functions, which represent the atomiclike absorption step functions, are related to the ionization potentials[21] associated with the excitation of $2p$ electrons to the unoccupied $3d$ states at the Ti site.

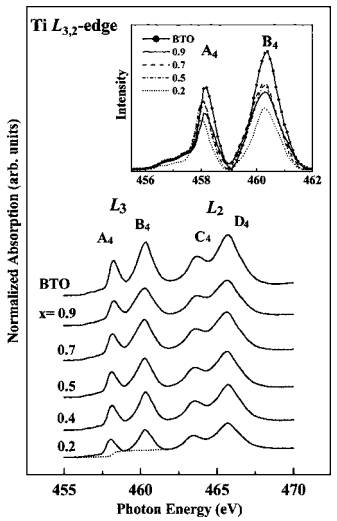

FIG. 5. Normalized Ti $L_{3,2}$-edge XANES spectra of B_xSTO. The inset presents the magnified A_4 and B_4 features after background subtraction.

The intensity decreases and the energy shifts to lower energies as x increases, suggesting that the effective charge of the Ti ion increases in P_xSTO. This finding reflects that Pb has a larger electronegativity than Ti (2.33 vs. 1.54),[15] so that there is electron transfer from Ti to Pb, which increases the positive effective charge of Ti. In contrast, the spectra of B_xSTO after background subtraction reveal that the intensity of the L_3-edge feature overall increases as the Ba content increases as shown in the inset of Fig. 5, which suggests that the Ti effective charge decrease with the increase of the Ba content. In this case, the decrease of the Ti effective charge reflects the smaller electronegativity of Ba than Ti (0.89 versus 1.54);[15] the direction of electron transfer is from Ba to Ti, which reduces the positive effective charge of Ti.

In summary, the XANES measurements provide direct evidence that the Pb–O bonding strongly affects O $2p$–Ti $3d$ hybridization in the TiO_6 octahedron of P_xSTO. In contrast, the Ba–O bonding does not substantially affect O $2p$–Ti $3d$ hybridization in B_xSTO. The Ti L_3-edge XANES spectra provide evidence of Pb-induced tetragonal distortion in the TiO_6 octahedron for $x \gtrsim 0.5$. In contrast, this effect is absent in B_xSTO.

This work was supported by National Science Council (NSC) of Republic of China under Contract No. NSC 93-2112-M-032-018.

[1]For example, see M. E. Lines, and A. M. Glass, *Principles and Applications of Ferroelectrics and Related Materials* (Clarendon, Oxford, 1979); J. F. Scott and C. A-Paz de Araujo, Science **246**, 1400 (1989).
[2]S. Piskunov, E. Heifets, R. I. Eglitis, and G. Borstel, Comput. Mater. Sci. **29**, 165 (2004).
[3]C. Kittel, *Introduction to Solid State Physics*, 7th ed. (Wiley, New York, 1996).
[4]R. E. Cohen, Nature (London) **358**, 136 (1992).
[5]B. Ravel, Ph.D. thesis, University of Washington, 1997.
[6]M. Imada, A. Fujimori, and Y. Tokura, Rev. Mod. Phys. **70**, 1039 (1998).
[7]K. Asokan, J. C. Jan, J. W. Chiou, W. F. Pong, M.-H. Tsai, H. L. Shih, H. Y. Chen, H. C. Hsueh, C. C. Chuang, Y. K. Chang, Y. Y. Chen, and I. N. Lin, J. Phys.: Condens. Matter **13**, 11087 (2001).
[8]J. C. Jan, K. Kumar, J. W. Chiou, H. M. Tsai, H. L. Shih, H. C. Hsueh, S. C. Ray, K. Asokan, W. F. Pong, M.-H. Tsai, S. Y. Kuo, and W. F. Hsieh, Appl. Phys. Lett. **83**, 3311 (2003).
[9]Y. H. Tang, M.-H. Tsai, J. C. Jan, and W. F. Pong, Chin. J. Phys. (Taipei) **41**, 167 (2003).
[10]S. Y. Kuo, C. T. Li, and W. F. Hsieh, Appl. Phys. Lett. **81**, 3019 (2002).
[11]S. Y. Kuo, W. Y. Liao, and W. F. Hsieh, Phys. Rev. B **64**, 224103 (2001).
[12]S. Y. Kuo, C. T. Li, and W. F. Hsieh, Phys. Rev. B **69**, 184104 (2004).
[13]Y. H. Tang and M.-H. Tsai (unpublished).
[14]F. M. F. de Groot, M. Grioni, J. C. Fuggle, J. Ghijsen, G. A. Sawatzky, and H. Petersen, Phys. Rev. B **40**, 5715 (1989).
[15]*Table of Periodic Properties of the Elements* (Sargent-Welch Scientific, Skokie, Illinois, 1980).
[16]Y. Kuroiwa, S. Aoyagi, A. Sawada, J. Harada, E. Nishibori, M. Takata, and M. Sakata, Phys. Rev. Lett. **87**, 217601 (2001).
[17]F. M. F. de Groot, M. Grioni, B. T. Thole, G. A. Sawatzky, and J. C. Fuggle, Phys. Rev. B **41**, 928 (1990).
[18]M. Abbate, R. Potze, G. A. Sawatzky, C. Schlenker, H. J. Lin, L. H. Tjeng, C. T. Chen, D. Teehan, and T. S. Turner, Phys. Rev. B **51**, 10150 (1995).
[19]J. P. Crocombette and F. Jollet, J. Phys.: Condens. Matter **6**, 10811 (1994).
[20]G. van der Laan, Phys. Rev. B **41**, 12366 (1990).
[21]J. Stöhr, *NEXAFS Spectroscopy* (Springer, Berlin, 1992), p. 231.